

RecNet: Early Attention Guided Feature Recovery

Subrata Biswas¹ Bashima Islam¹

Abstract

Uncertainty in sensors results in corrupted input streams and hinders the performance of Deep Neural Networks (DNN), which focus on deducing information from data. However, for sensors with multiple input streams, the relevant information among the streams correlates and hence contains mutual information. This paper utilizes this opportunity to recover the perturbed information due to corrupted input streams. We propose RecNet, which estimates the information entropy at every element of the input feature to the network and interpolates the missing information in the input feature matrix. Finally, using the estimated information entropy and interpolated data, we introduce a novel guided replacement procedure to recover the complete information that is the input to the downstream DNN task. We evaluate the proposed algorithm on a sound event detection and localization application where audio streams from the microphone array are corrupted. We have recovered the performance drop due to the corrupted input stream and reduced the localization error with non-corrupted input streams.

1. Introduction

On-device deep learning has attracted the interest of researchers with the growth of mobile and IoT devices (Lane et al., 2017; Chen et al., 2020). These devices use sensors to collect the data and pass these sensor streams as inputs to a deep neural network (DNN) for inference. Most DNNs process inputs of constant dimensions (Li et al., 2020b) and perform poorly with missing or corrupted portions in inputs (Roy et al., 2020; Yin & Hou, 2016). Such data corruption occurs due to uncertainty, e.g., unstable communication medium (Hyadi et al., 2016), stochastic energy (Islam & Nirjon, 2020), and sensor failure (Li et al., 2020a).

Though statistical methods (Jerez et al., 2010) like mean imputation (Allison, 2001), hot deck (Little & Rubin, 2019), and multiple imputations (Rubin, 1996) can recover missing data portions, these imputation techniques fail whenever the missing data sequence is long (Hasan et al., 2021). Besides, the statistical feature is insufficient for higher dimensional and complex data distributions in real-world applications (Al-Janabi & Alkaim, 2020), including image processing, acoustic sensing, and RF imaging. Therefore, there is a need for more sophisticated techniques for recovering or proxying these missing/corrupted input data to avoid erroneous DNN inference output.

Multiple input streams are used in many real-world applications, including speaker separation (Nugraha et al., 2016), vehicle localization (de Godoy et al., 2018), cybersecurity (Jiang et al., 2018), seizure detection (Yuan et al., 2018), and emotion recognition (Chao et al., 2018). These multiple input streams produce high-dimensional data, which gets corrupted if any sensor stream malfunctions. Such data perturbation often leads to performance degradation.

One example of DNN tasks with higher dimensional and complex data is sound source localization with a microphone array. Sound source localization is a significant and challenging component of various applications, including augmented and virtual reality (Ahrens et al., 2019), robotics (Argentieri et al., 2015), virtual assistants (Rahaman & Kim, 2021), and pedestrian safety (de Godoy et al., 2018). A sound originating from the source propagates through the medium and reaches the spatially separated mics of a microphone array at different times and phases. Signal processing (Schmidt, 1986; DiBiase, 2000; Roy & Kailath, 1989) and deep learning-based (Xiao et al., 2015; Yalta et al., 2017; Chakrabarty & Habets, 2017) solutions to estimate the degree of arrival (DOA) utilizes these temporal and spatial differences of the received signals.

Literature shows that providing complex features, e.g., generalized cross-correlation, spectral power, and phase spectrum, as the input significantly improves the classification or regression performance of a DNN compared to raw time-domain input (Rajanna et al., 2015). Any input stream corruption pollutes the generated features and causes poor DNN inference performance. Due to the stochasticity and randomness of missing data, more than simply simulating

¹Department of Electrical and Computer Engineering, Worcester Polytechnic Institute, Massachusetts, USA. Correspondence to: Subrata Biswas <sbiswas@wpi.edu>, Bashima Islam <bislam@wpi.edu>.

the probable scenarios or augmenting the data is required.

Understanding the relationship between multiple variables is one of the essential objectives of deep learning. Mutual information and conditional entropy can quantify the relationship between the variables (Vergara & Estévez, 2014). Although it is challenging to determine these underline relationships, recent developments in deep learning show tremendous success in information estimation (Hjelm et al., 2018; Poole et al., 2019). These estimated relationships present the opportunity to recover the corrupted data.

By exploiting this opportunity, this paper combines information entropy estimation and conditional interpolation to recover the inference performance loss due to missing and corrupted data streams. First, we propose an early attention model (EA) that estimates the available information and information entropy at each element or unit of the calculated features to understand the effect of the corrupted data stream on that element. Next, our deep conditional interpolator (DCI) to estimate missing information content utilizing the estimation relation. Finally, the information entropy from the EA guides a replacement protocol of the affected element from the initially generated features with the interpolated features from DCI without impacting the element unaffected by corrupted data. This newly replaced feature enters the DNN model (down-stream task) for inference.

This paper implements and evaluates the proposed algorithm for a sound event detection and localization downstream task and achieves 22.80%, 34.21%, and 18.77% performance recovery compared to the baseline, data stream averaging, and correlation-based data stream duplication, respectively. We further achieve $36.91 \pm 3.56\%$ less degree of arrival error from downstream tasks trained with a corrupted dataset.

2. Theory

This section formulates the problem and provides the mathematical foundation of the proposed solution.

Let us consider X as the raw data dependent on a set of n random variables, $S = \{x_1, x_2, \dots, x_n\}$. Then X can be represented by

$$X = f(S) \quad (1)$$

Extracted features perform better than raw data as input to a DNN when a large training corpus is absent. Raw domain data, X , is mapped to the feature domain data, F , by a feature extraction function, G . Thus, $F = G(X)$.

Note that, though recent embedding DNNs take raw features as input and output higher dimensional features to provide a performance boost (Schneider et al., 2019), these DNN models will also suffer from corrupted data streams.

Since F is a function of X , and X depends on a set of random variables (S), the amount of information content or

entropy, i , at every element of F depends on the same set of random variables, S . Thus the information entropy at the k^{th} element of F , i_k , can be formulated as

$$i_k = -G(f(S_k) \log G(f(S_k)) \quad (2)$$

i_k is a real number, and $i_k \in [0, 1]$. $i_k = 1$ represents the presence of all information, while $i_k = 0$ indicates a complete absence of information. Any value between 0 and 1 implies *fractional missing information (FMI)* and quantifies the amount of missing information in the feature map F when observed data is low-rank, \tilde{X} , compared to hypothetical full-rank data, X . This rank deficiency occurs when one or some element of set S is missing or corrupted. Thus, low-rank \tilde{X} produces rank-deficient \tilde{F} .

Orchard et al. introduced the computation principle of FMI (Orchard & Woodbury, 1972), which states that the likelihood of complete data, $L(\theta|X)$, can be factored into the likelihood of the observed lower-ranked data, $L(\theta|\tilde{X})$, and the density of rank-deficient data given the observed data, $f(Z|\theta, \tilde{X})$, where Z and θ are missing data and model parameter, respectively.

$$L(\theta|X) = L(\theta|\tilde{X})f(Z|\theta, \tilde{X}) \quad (3)$$

The first derivative of the complete data log-likelihood can be represented as

$$\frac{\partial \log L(\theta|X)}{\partial \theta} = \frac{\partial \log L(\theta|\tilde{X})}{\partial \theta} + \frac{\partial \log f(Z|\theta, \tilde{X})}{\partial \theta} \quad (4)$$

The covariance matrix of equation 4 defines the information matrix, J_X , which is derived by the following equation–

$$J_X = Cov\left(\frac{\partial \log L(\theta|X)}{\partial \theta}\right); \quad J_{\tilde{X}} = Cov\left(\frac{\partial \log L(\theta|\tilde{X})}{\partial \theta}\right); \\ J_{X|\tilde{X}} = Cov\left(\frac{\partial \log f(Z|\theta, \tilde{X})}{\partial \theta}\right)$$

Here, $Cov(\cdot)$ is the covariance. Finally, equation 4 can be written as

$$J_X = J_{\tilde{X}} + J_{X|\tilde{X}} \quad (5)$$

In summary, complete information J_X can be written as a sum of available low-rank information $J_{\tilde{X}}$ and $J_{X|\tilde{X}}$ missing information matrix.

The rank-deficient \tilde{F} consists of two components, information content and noise content. The latter arises due to the missing elements of S . Hence, the information content, $J_{\tilde{X}}$, can be written in terms of \tilde{F} as equation 6, here I is the element-wise information entropy of \tilde{F} . So, the missing information matrix $J_{X|\tilde{X}}$ can be obtained by estimating the values of the missing elements in noise contents from the existing information contents. If \hat{F} is the estimated

missing information then $J_{X|\tilde{X}}$ is presented by equation 7.

$$J_{\tilde{X}} = I \otimes \tilde{F} \quad (6) \quad J_{X|\tilde{X}} = (1 - I) \otimes \hat{F} \quad (7)$$

With equation 6 and 7, equation 5 can be written as

$$J_X = I \otimes \tilde{F} + (1 - I) \otimes \hat{F} \quad (8)$$

3. Proposed Methodology

Our proposed model maps the low-ranked feature matrix into the full-ranked feature matrix by estimating the missing information matrix for a given task using a three-step approach. Figure 1 shows the overall architecture of the proposed model. Our proposed model sits between the feature extraction module and the downstream task (DT), which is application dependant and is defined by the application. Note that this paper does not have any contribution to these modules. Our proposed architecture consists of three main components – early attention (EA), deep conditional interpolator (DCI), and guided replacement (GR). EA estimates the low-rank information and measures the element-wise information entropy (I in Equation 6). At the same time, DCI interpolates the missing elements (\hat{F} in Equation 7) from the available low-rank feature matrix. Finally, GR combines the less informative elements of the original feature set with the interpolated feature values in the guidance of element-wise information entropy. This combining process is governed by the equation 8. The resultant enhanced feature set is fed to the downstream task for inference.

3.1. Early Attention

This step aims to estimate the information entropy, I , for each element of the low-rank feature set \tilde{F} . To achieve this, we design an early attention step that estimates the channel and spatial information entropy (Park et al., 2018). The left-hand side of Figure 1 shows the details of the proposed early attention architecture.

Low-rank feature set $\tilde{F} \in \mathbb{R}^{d_{\tilde{X}}}$ is the input to the EA, where $d_{\tilde{X}}$ is the dimension of \tilde{F} . The first component of EA is the channel information branch, $f_{\gamma}(\tilde{F})$. Here we parameterize the channel information branch with γ . This branch performs average pooling, followed by a multi-layer perception (MLP) on the input to extract the channel information entropy. Average pooling feeds gradients across all indices and thus enables the model to learn more robust features while more accurately depicting the overall strength of a feature. At this point, we expand the feature by an expansion factor, e . The MLP consists of three fully connected layers with batch normalization and rectified linear unit (ReLU) after the first two layers. Finally, this branch outputs a vector I_c that measures of global information on each channel.

The second component of EA is the point-wise information branch, $f_{\lambda}(\tilde{F})$. The parameters of the point-wise informa-

tion branch is represented by λ . The input, \tilde{F} , first passes through a convolution layer with a kernel size of (1×1) and a channel reduction factor of r . Then it goes through n number of dilated convolution layers with a kernel of (3×3) with dilation value d , batch normalization, and ReLU activation. In our architecture, $n = 3$ and $d = 2$. The dilated convolution increases the respective field and enables us to leverage contextual information. Finally, this contextual information passes through another convolutional layer of kernel size (1×1) and outputs I_s , which estimates the point-wise information of the input feature.

$$I_c = f_{\gamma}(\tilde{F}) \quad (9) \quad I_s = f_{\lambda}(\tilde{F}) \quad (10)$$

Next, we broadcast I_s to $\mathbb{R}^{d_{\tilde{X}}}$ to get information entropy estimation of the same dimension as \tilde{F} and perform element-wise addition on I_c and I_s . Element-wise addition ensures smooth gradient flow (He et al., 2016). Finally, we pass it through a sigmoid function that maps the results between 0 and 1, where a value closer to 1 indicates higher information availability and vice versa.

$$J_{\tilde{X}} = (1 + \sigma(I_c + I_s)) \otimes \tilde{F} \quad (11)$$

Here, \otimes denotes element-wise multiplication, $(1 + \sigma(I_c + I_s))$ is the information entropy, I , and σ is sigmoid function.

3.2. Deep Conditional Interpolator

The deep conditional interpolator (DCI), $f_{\beta}(\tilde{F})$, estimates the missing information by exploiting relations among the available channels. DCI is parameterized by β . The right-hand side of Figure 1 shows the architecture of DCI. It takes \tilde{F} as input and provides interpolated feature \hat{F} as output. Thus, $\hat{F} = f_{\phi}(x_j | x_1, x_2, \dots, x_{j-1}, x_{j+1}, \dots, x_n)$. Here, x_j is the corrupted or missing data stream. We propose a function f_{ϕ} that takes the low-rank feature and interpolates it to reach its full-rank. We choose an auto-encoder (AE) for estimating f_{ϕ} . AE is a robust framework that can learn compressed intermediate representation and commonly use this intermediate result to reconstruct the input. Moreover, AE semantically mixes characteristics from data and performs as an efficient interpolator (Berthelot et al., 2018).

DCI contains one contraction and one expansion path. The contraction path has n consecutive downsampling blocks, where each block is formed by a convolution layer followed by a rectified linear unit and batch normalization. In our implementation, $n = 5$, kernel size is 5×3 , and the RELU slope is 0.2. Using a stride of 2, we downsample the feature on each step. However, we double the number of output feature channels after each downsampling block. The output of the contraction path is $F_{con} \in \mathbb{R}^{d_c}$, where F_{con} stands for the latent intermediate representation of the input feature set, \tilde{F} , and d_c represents the intermediate feature dimension.

The expansion path passes the input F_{con} through 5 consecu-

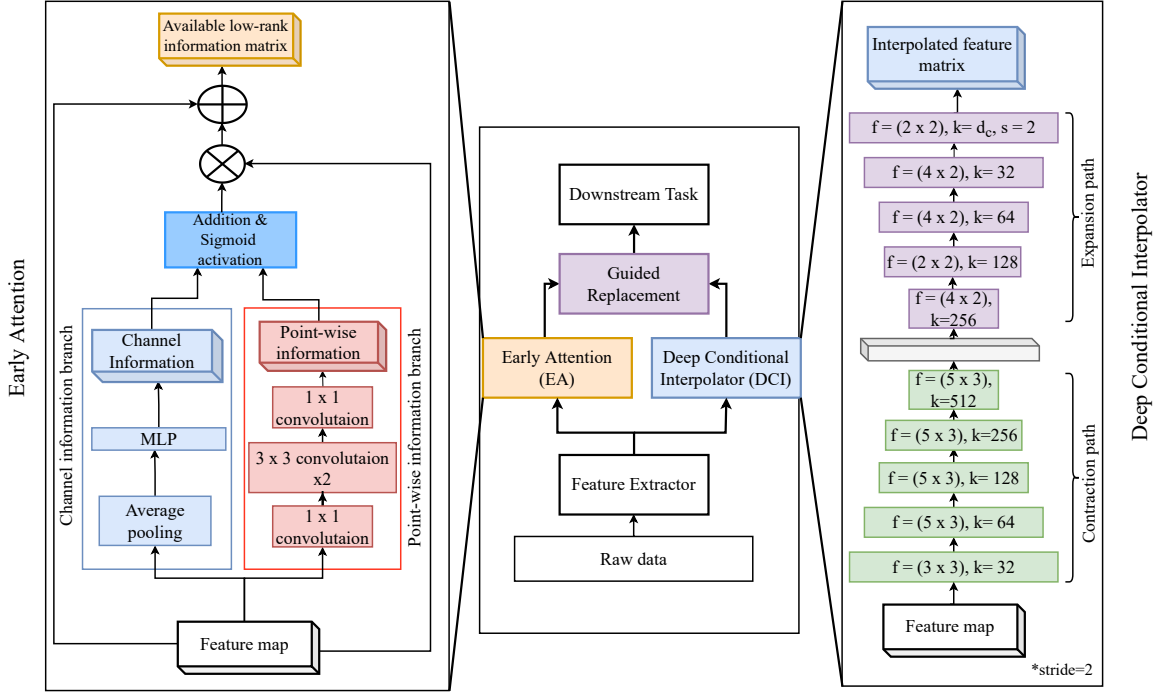


Figure 1: Architecture of proposed RecNet. Note that only the highlighted components are the contributions of this paper.

tive upsampling blocks consisting of transposed convolution layers (kernel = 4×2 or 2×2 and stride = 2) with batch normalization and leaky-ReLU activation. The last convolution has a sigmoid activation and skips on batch normalization. After each up-sampling block, we half the number of output feature filters and set the last layer’s output filter number to match the shape of the input feature map. The expansion path returns the interpolated feature matrix, $\hat{F} \in \mathbb{R}^{d_z}$.

$$\hat{F} = f_{\beta}(\tilde{F}) \quad (12)$$

3.3. Guided Replacement

We replace the low-rank \tilde{F} with the interpolated feature \hat{F} . The whole replacement process is guided by I_s . The k^{th} element I_s provides the amount of available information present at the k^{th} element of \tilde{F} . $f_{\beta}(\cdot)$ is designed to establish equivalency between $(1 - I)f_{\beta}(\tilde{F})$ and $(1 - I_s)f_{\beta}(\tilde{F})$. Hence, $J_{X|\tilde{X}}$ can be quantified as follows

$$J_{X|\tilde{X}} = (1 - I_s) \otimes \hat{F} \quad (13)$$

We utilize the low-rank information matrix, $J_{\tilde{X}}$, and missing information matrix, $J_{X|\tilde{X}}$, to find the estimated full-rank enhanced feature matrix J_X from equation 5.

3.4. Training

We train our proposed architecture jointly with the downstream task (DT). Let us assume that the loss function of DT is \mathcal{L}_{DT} . The impact of this loss, \mathcal{L}_{task} , backpropagates

through DT as well as the channel and point-wise information branches (f_{γ} and f_{λ}) of EA. However, DCI (f_{β}) has a separate training loss, \mathcal{L}_{DCI} , the squared L_2 distance between F and \hat{F} . \mathcal{L}_{DCI} is defined by $\mathcal{L}_{DCI} = \|F - \hat{F}\|^2$. Note that we use two different optimizers to train the DT and EA with \mathcal{L}_{DT} and DCI with \mathcal{L}_{DCI} separately.

4. Experimental Setup

This section describes the dataset, feature extraction, downstream task, baseline, data preparation, and evaluation metrics to evaluate RecNet for sound event detection and localization. Our implementation can be found at ¹

4.1. Dataset & Feature Extraction

Dataset. We use the DCASE2021 challenge Task 4 dataset (Politis et al., 2021) to evaluate our proposed algorithm. This challenge aims to detect sound events and localize sound sources regarding the degree of arrival (DoA). The dataset contains 600 4-channel 1-minute spatial recordings of overlapping sound events sampled at 24KHz. We have 400 samples in the development set, and the rest of the 200 constitutes the evaluation set. DCASE takes 12 different sound event classes from the NIGENS general sound event dataset (Trowitzsch et al., 2019), which has 14 classes. This dataset contains directional interference where some sound events in the recordings are not present in the target

¹<https://github.com/hidethyself/RecNet-ICML2023>

classes. A group of spatial room impulse responses (SRIR) determines the synthesis of these spatial recordings, and a maximum of 4 polyphony can be present in each recording. Moreover, multi-channel ambient noise is also present where the noise level is scaled in signal-to-noise-ratio (SNR) and is randomly taken from 6dB to 30dB.

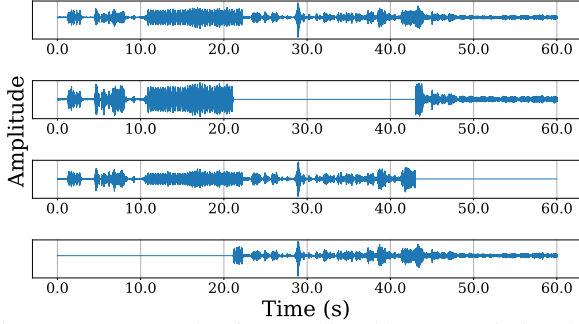


Figure 2: An example of raw audio with 100% missing data. **Feature Extraction.** Following the provided feature extraction procedure of the challenge, we first, perform 1024-point FFT with a 40 ms window length and 20 ms hop length at 24 kHz on the raw time-domain audio data. We take the multi-channel log-Mel-spectrogram from the FFT results in 64 Mel bands. Next, we calculate the generalized cross-correlation (GCC) from the raw audio and truncate the GCC sequences to the same value as the Mel bins. Finally, we stack these two features to obtain the feature matrix, F .

4.2. Downstream Task

The downstream task (DT) in this evaluation is we choose sound event detection and localization (SELD). We opt for SELD since it comprises two tasks: sound event detection (SED) and sound event localization (SEL). SEL requires multi-channel audio as it utilizes the spatial relationship among microphones. On the other hand, SED algorithms only require the amplitude information of the audio signal; hence mono-channel audio signal suffices. We can consider each channel of this audio signal as a random variable, x_i , and an element of set \mathcal{S} . Similarly, multi-channel audio as raw data, X , is a function of set \mathcal{S} . Thus, any corrupted element in \mathcal{S} results in a low-rank feature matrix \tilde{F} .

DT is primarily trained with the full-rank feature matrix, F , and the loss function, \mathcal{L}_{DT} . To deploy proposed algorithm, we retrain DT with the feature matrix, J_X , which is recovered from the low-rank feature matrix \tilde{F} .

We employ the SELD algorithm from (Adavanne et al., 2018; Shimada et al., 2021) to develop our downstream task model. This model uses an activity-coupled Cartesian DOA (ACCDOA) representation, which assigns a sound event activity to the length of a corresponding Cartesian DOA vector. The SELD task is converted into an ACCDOA estimation problem. The model comprises a convolutional recurrent neural network (CRNN) (Cao et al., 2019) followed by a

single full-connected (FC) layer, which estimates the ACCDOA representation vector. The CRNN model has multiple 2D CNN layers with ReLU and batch normalization to learn local shift-invariant features from the spectrograms. Filter kernels spanning all channels allows CNN to learn inter-channel features. Moreover, max-pooling of size two is used to reduce dimensionality after each CNN block.

4.3. Data Preparation

We randomly select a channel to emulate the missing audio channel and replace the original audio with Gaussian noise of 0 mean with a standard deviation of 1. We assume that up to 50% of the channels can miss data anytime. In our experimental setup with four microphones, the number of missing channels belongs to the set $[0, 1, 2]$. A $p\%$ missing data percentage (MDP) denotes that $p\%$ of the total length of audio is corrupted with noise. We randomly distribute the length of missing data among all available channels. To reduce bias, we conduct all experiments with the MDP 5 times with different random seeds and report the mean and variance. Figure 2 shows an example raw audio where MDP is 100% and only 1 channel is missing channel at any time.

4.4. Baseline

To evaluate the performance of our proposed algorithm, we compare it against five baselines.

Full-Rank Model (FR). In this model, we train DT with the full-rank feature matrix, F , and the missing data percentage (MDP) is 0%. Thus, there is no missing information.

Low-Rank Model (LR_p). We train DT with the \tilde{F} and $p\%$ MDP. Here, LR_{75} denotes 75% MDP.

Correlation Replacement Low-Rank Model (CLR_p). This model first works on the raw audio data to compensate for the low-rank feature matrix. We replace the gaussian noises of the missing channel with the data from the most correlated channel. Then we calculate the feature and pass it through a DT model trained with $p\%$ MDP.

Average Replacement Low-Rank Model (ALR_p). This model manipulates the raw data similarly to CLR_p . However, instead of replacing the noise with the most correlated channel, it uses the average of all available channels.

Reduced Channel Full-Rank Model (R_nFR). In this case, we assume that $(n-k)$ channels are available and MDP is 0%. In our implementation, $n = 4$ and $k = 1$. This model shows the effect of having a smaller n with 0% MDP on the SELD task. Here, we train DT with the full-rank matrix, F .

4.5. Evaluation Metrics

We evaluate the sound event detection (SED) and degree of arrival (DoA) estimation performance with four metrics. We use error rate (ER_{SED}) and $F1$ -score to evaluate SED estimation for each one-second audio segment (Mesaros et al., 2016; Virtanen et al., 2018). In ideal cases, ER_{SED} is zero while $F1$ -score is one. The DoA error (E_{DoA}) and localization recall (R_L) evaluated localization performance.

Event Detection Error Rate (ER_{SED}) is represented by the following equation –

$$ER_{SED} = \frac{\sum_{k=1}^K S(k) + \sum_{k=1}^K D(k) + \sum_{k=1}^K I(k)}{\sum_{k=1}^K N(k)} \quad (14)$$

Here, $N(K)$ is the total number of active sound events present in the reference for each one second segment k , $S(K)$ represents the number of events detected with the wrong label, $I(k)$ stands for insertions, $D(k)$ deletions. These statistics can be defined as –

$$\begin{aligned} S(k) &= \min(FN(k), FP(k)) \\ D(k) &= \max(0, FN(k) - FP(k)) \\ I(k) &= \max(0, FP(k) - FN(k)) \end{aligned}$$

Here, for the k^{th} one-second segment, $TP(k)$ is the total number of sound events present in both prediction and reference, $FP(k)$ represents the number of active sound events in prediction but inactive in reference, $FN(k)$ stands for the number of sound events inactive in the prediction.

Event Detection F1-score ($F1$) is defined as follows

$$F1 = \frac{2 \sum_{k=1}^K TP(k)}{2 \sum_{k=1}^K TP(k) + \sum_{k=1}^K FP(k) + \sum_{k=1}^K FN(k)} \quad (15)$$

Degree of Arrival Estimation Error (E_{DoA}) of entire dataset is represented by the following equation.

$$E_{DoA} = \frac{1}{D} \sum_{d=1}^D \zeta((x_e^d, y_e^d, z_e^d), (x_r^d, y_r^d, z_r^d)) \quad (16)$$

Here, (x_e, y_e, z_e) and (x_r, y_r, z_r) are the estimated and reference coordinates, respectively. ζ is the angle between the reference and estimated coordinates and is calculated as $\zeta = 2 \arcsin\left(\frac{\sqrt{(x_r - x_e)^2 + (y_r - y_e)^2 + (z_r - z_e)^2}}{2}\right) \frac{180}{\pi}$.

Localization Recall (R_L) measures the localization performance on each frame. LR is represented by

$$R_L = \frac{TP_{DoA}}{TP_{DoA} + FN_{DoA}} \quad (17)$$

Here, TP_{DoA} stands for total number of the time frames where number of estimated DoAs is equal to the number of reference DoAs, and FN_{DoA} represents the total number of time frames where estimated and reference DoAs are not equal. We consider DoA prediction as a true positive if it's distance is within 20° .

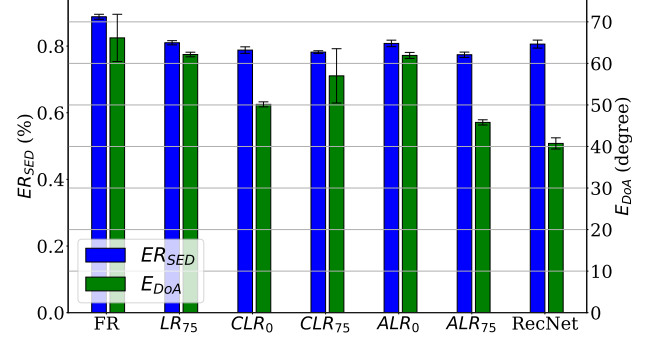


Figure 3: Performance of the baselines and RecNet.

5. Results

This section provides the results of our experiments.

5.1. Comparison with Baseline

Figure 3 compares the SED and DoA estimation errors (ER_{SED} and E_{DoA}) among different classical data replacement techniques and our proposed, RecNet, for inference data with 75% MDP. We observe that all models trained with full rank features, e.g., FR , CLR_0 , and ALR_0 , experience the highest SED and DoA error. However, when trained with corrupted data with 75% MDP, LR_{75} , CLR_{75} , and ALR_{75} , achieves 8.78%, 0.76%, 4.20% and 6.04%, 13.68%, 26.03% less ER_{SED} and E_{DoA} than the the full-ranked versions, respectively. RecNet has 11.04 – 38.40% lower E_{DoA} than the rest. We notice a higher DoA estimation gain due to DoA's dependency on phase information for calculating the time-of-arrival. Thus, training with MDP data provides a robust model that can endure missing data.

Though classic replacements (CLR and ALR) improved significantly, RecNet achieves up to 34.22% less E_{DoA} than the other models with 75% MDP. Unlike classical approaches that fail to recover phase information, RecNet considers both channel and spatial information. Besides, RecNet does not require prior knowledge of which mic is corrupted, which is essential for classic replacement models. RecNet has 38.40% higher ER_{SED} than CLR_{75} and ALR_{75} as a single mic is often sufficient for SED.

Figure 6 observes cases where a single input stream (mic) is completely missing. R_3FR , where full-rank input from three mics is used in training and testing, has 6.29% lower E_{DoA} than LR_{100} . However, RecNet reduces the E_{DoA} by 67.59%. In Table 1 when $MDP = 0$, which means training on full-rank features domain, RecNet achieves 22.80% of gain in E_{DoA} while gaining 1.33% in ER_{SED} . Thus, RecNet boosts the performance for the full-rank feature too.

5.2. Effect of Missing Data Percentage (MDP)

Table 1 shows the performance of RecNet and the low-rank model for a set of MDP with $p = 10, 25, 50, 75, 100\%$. We

Table 1: SELD performance of different model configurations. LR_p denotes the DT is trained with $p\%$ MDP.

MDP	Method	E_{SED}	$F1$	E_{DoA}	R_L
0	$FR(LR_0)$	0.76	16.90	42.10	34.70
	RecNet	0.75	18.10	32.50	39.80
10	LR_{10}	0.77	14.30	59.60	32.00
	$LR_{10} + EA$	0.75	16.20	33.70	38.50
	$LR_{10} + DCI$	0.84	9.50	41.10	28.10
	$LR_0 + EA$	0.80	10.90	48.00	27.00
	$LR_0 + EA + DCI$	0.80	10.10	47.60	26.60
	RecNet	0.75	17.50	35.10	38.20
25	LR_{25}	0.79	14.70	59.10	30.70
	$LR_{25} + EA$	0.78	13.70	49.10	35.00
	$LR_{25} + DCI$	0.84	6.60	54.10	24.30
	$LR_0 + EA$	0.83	8.20	55.20	21.70
	$LR_0 + EA + DCI$	0.83	7.70	66.30	22.40
	RecNet	0.78	13.90	35.90	34.60
50	LR_{50}	0.81	10.30	63.30	26.50
	$LR_{50} + EA$	0.80	12.50	50.40	30.80
	$LR_{50} + DCI$	0.86	6.40	51.10	23.70
	$LR_0 + EA$	0.88	4.70	72.70	15.30
	$LR_0 + EA + DCI$	0.88	4.30	61.00	15.80
	RecNet	0.79	13.40	43.00	33.80
75	LR_{75}	0.82	11.40	61.90	26.10
	$LR_{75} + EA$	0.79	11.30	53.40	31.50
	$LR_{75} + DCI$	0.86	5.20	58.20	24.10
	$LR_0 + EA$	0.91	1.70	85.50	11.70
	$LR_0 + EA + DCI$	0.90	2.40	82.70	12.80
	RecNet	0.77	17.00	36.90	37.40
100	LR_{100}	0.82	9.10	67.20	25.90
	$LR_{100} + EA$	0.79	11.20	53.90	32.10
	$LR_{100} + DCI$	0.84	6.90	56.20	26.50
	$LR_0 + EA$	0.92	2.60	84.30	11.40
	$LR_0 + EA + DCI$	0.90	1.50	92.60	13.50
	RecNet	0.79	12.80	41.10	32.60

observe that RecNet achieves $2.49 \pm 0.76\%$ and $36.91 \pm 3.56\%$ degree lower in both ER_{SED} and E_{DoA} than LR_p , respectively. Besides, the E_{DoA} of LR_p significantly increases with lower available information or higher p since spatial relationships among different input streams are the most critical feature for localization tasks. On the other hand, RecNet maintains its performance with 0.02 and 3.16 variance in SED and DoA errors consecutively.

5.3. Effect of Different Model Configurations

Figure 4 and 5 shows the performance deviation for ER_{SED} and E_{DoA} when only EA , DCI , or pre-trained (FR_0) models are used compared to RecNet. It is noticeable that RecNet performs significantly better than the rest.

Effect of EA. Figure 4 shows that integrating and jointly training EA only ($LR_p + EA$) with the DT trained with low-rank (LR_p) reduces E_{DoA} by $22.85 \pm 10.56\%$. In Table 1, we see that the accuracy and F1-score for SED increase only by $2.48 \pm 1.08\%$ and $10.01 \pm 11.92\%$ for EA. Though adding EA with DT improves the performance, it can only estimate the available information entropy at each element of the

feature matrix, \tilde{F} . As it can not estimate that element's value in the full-rank version. F , the performance is lower than a full-rank system (FR_0) where MDP is 0% during inference (Figure 5). Thus, RecNet with DCI to estimate the feature values have $16.76 \pm 11.21\%$ and $-0.003 \pm 0.79\%$ less E_{DoA} and ER_{SED} than $LR_p + EA$ (Figure 4). In Figure 5, RecNet further achieves $4.68 \pm 7.69\%$ less E_{DoA} than FR_0 with full-rank inference feature.

Effect of DCI. In Figure 4 and 5, only adding DCI reduced E_{DoA} by $16.22 \pm 8.87\%$ compared to only DT. However, this error is still $23.99 \pm 7.69\%$ and $26.55 \pm 14.56\%$ higher than RecNet and FR . Only DCI with DT's ($LR_p + DCI$) performance is lower because when DCI estimates the full-rank features (\hat{F}), it adds error to the matrix elements where the effect of missing data is minimal. This additional error increases the ER_{SED} by $11.57 \pm 1.29\%$ as the missing phase information is less critical for SED. EA provides the information entropy and reduces this additional error. Utilizing EA and DCI, RecNet replaces the low-rank feature with the guidance of estimated information entropy. Figure 7 shows an example of the low-rank and estimated full-rank features. Thus, RecNet performs better than the rest.

Effect of Re-Training DT. Figure 4 and 5, if we freeze the weights of the re-trained DT with its pre-trained version ($FR_0 + EA$ and $FR_0 + EA + DCI$), which is trained with the full rank matrix, E_{DoA} significantly increases by $23.99 \pm 7.50\%$ and $77.54 \pm 34.23\%$ from the re-trained version $LR_p + EA$ and RecNet, respectively. This result indicates that EA and DT joint training is necessary for EA to learn the element-wise information entropy better, which is critical for the successful replacement of low-rank feature.

5.4. Effect of Simultaneously Missing Input Streams.

In Figure 8, we compare two systems where the number of simultaneously missing input streams is one and two, respectively. As anticipated, the system with missing information from a single stream performs better than the one with two missing streams due to the lack of available information for estimation. Though missing two streams results in 46.18% less E_{DoA} than a single missing stream for 50% MDP, with higher MDP, the E_{DoA} for two missing input streams increases significantly. With more unavailable input streams, the information entropy estimation becomes more inexact, and the guided replacement becomes inaccurate.

6. Related Work

The mutual information between the input and output of each layer quantifies DNN (Colombini et al., 2014). This information is hard to understand as we only have the data samples but not the distributions (McAllester & Stratos, 2020). Previously proposed optimizers solve the tasks with

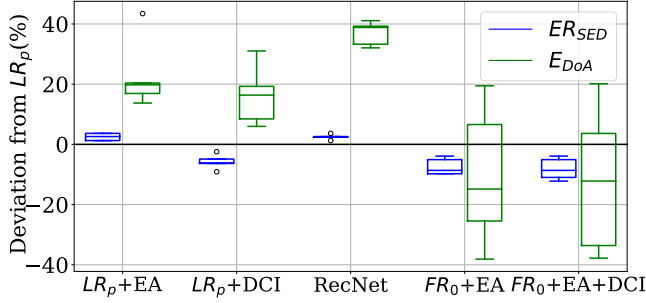


Figure 4: Deviation of ER and DoA_{err} from LR_x for different model configurations.

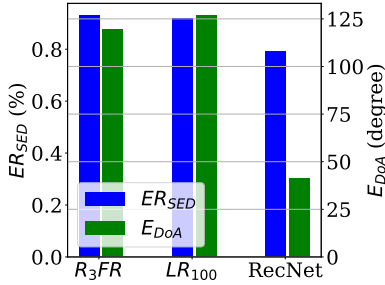


Figure 6: Performance when one data stream is completely missing.

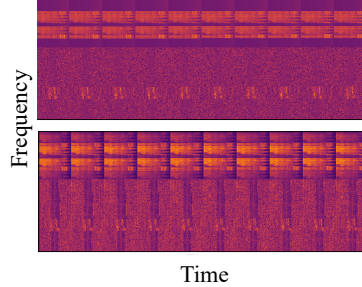


Figure 7: Example of low-rank (top) and estimated full-rank (bottom) features.

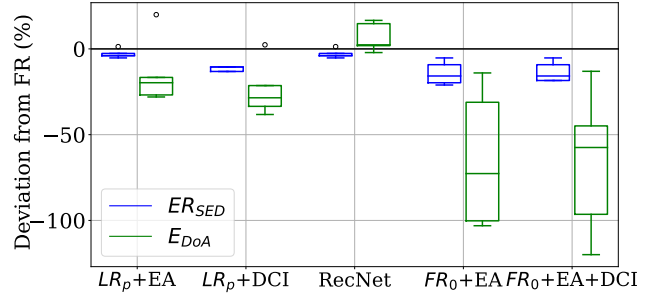


Figure 5: Deviation of ER and DoA_{err} from FRM for different model configurations.

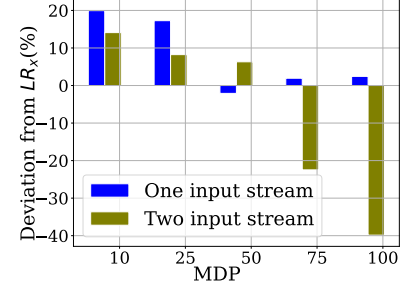


Figure 8: Effect of simultaneously missing input streams.

minimal information on input distribution (Aleml et al., 2016) but do not address corrupted data samples.

Attention learns the cognitive and behavioral characteristics to focus on essential information and ignore identifiable features selectively (Colombini et al., 2014). For multi-channel input, attention explores the channel characteristics and estimates the channel state information (Gao et al., 2021). Though commonly used later in a network, using attention early improves performance with substantial margins (Hajavi & Etemad, 2020) motivating our EA component.

Autoencoders have shown significant success as interpolators and are used as qualitative experimental outcomes and latent variable generational models (Dumoulin et al., 2016; Ha & Eck, 2017). Autoencoders can also successfully extrapolate beyond the training data (Carter & Nielsen, 2017). Therefore, we use an autoencoder as an interpolator in DCI.

Missing multi-stream data has been used to attain better performance on tasks such as speech enhancement (Taherian et al., 2022). However, speech enhancement is only partially dependent on spatial information, which is harder to recover. Some recent works focus on recovering missing modalities in multimodal sensing (Ma et al., 2022; 2021).

Sound event detection (SED) with overlapping sound events is known as polyphonic SED. Several traditional approaches, including the Gaussian mixture Model (GMM) and Hidden Markov Model (HMM) (Mesaros et al., 2010), along with deep learning (DL) approaches (Cakir et al., 2015; Phan et al., 2016; Zhang et al., 2015; Parascandolo et al.,

2016), have been explored for this classification problem. Recent works show that convolutional-recurrent neural networks (CRNN) perform better than the earlier DL approaches (Cakir et al., 2017; Lim et al., 2017), and thus we utilize it as our downstream task.

Classic sound source localization (SSL) methods, e.g., MUSIC (Gupta & Kar, 2015), independent component analysis (Sawada et al., 2003; Noohi et al., 2013), and sparse models (Yang et al., 2018), perform poorly for under-determined scenarios. Recently DNN has shown promising results for SSL (Ferguson et al., 2018; Yiwere & Rhee, 2017), especially when SED and SSL are jointly trained as a sound event detection and localization (SELD) task (Hirvonen, 2015). This joint training overcomes data association problems between estimated DOAs and detected sound events. Thus, we choose SELD over only SSL.

7. Discussions and Limitations

Interdependence among different random variables can be utilized to recover missing information. Though many classical algorithms exist to handle missing data points, they suffer due to their limitations, e.g., the requirement of prior knowledge and performance degradation on high and complex data distributions. This paper shows how to overcome such limitations. However, the proposed method requires training the downstream task to gain performance. Also, we have minimal improvement for the task where multiple data stream is optional. We will focus on removing the downstream task retraining requirement in our future work.

References

- Adavanne, S., Politis, A., Nikunen, J., and Virtanen, T. Sound event localization and detection of overlapping sources using convolutional recurrent neural networks. *IEEE Journal of Selected Topics in Signal Processing*, 13(1):34–48, 2018.
- Ahrens, A., Lund, K. D., Marschall, M., and Dau, T. Sound source localization with varying amount of visual information in virtual reality. *PloS one*, 14(3):e0214603, 2019.
- Al-Janabi, S. and Alkaim, A. F. A nifty collaborative analysis to predicting a novel tool (drfls) for missing values estimation. *Soft Computing*, 24(1):555–569, 2020.
- Alemi, A. A., Fischer, I., Dillon, J. V., and Murphy, K. Deep variational information bottleneck. *arXiv preprint arXiv:1612.00410*, 2016.
- Allison, P. D. *Missing data*. Sage publications, 2001.
- Argentieri, S., Danes, P., and Souères, P. A survey on sound source localization in robotics: From binaural to array processing methods. *Computer Speech & Language*, 34(1):87–112, 2015.
- Berthelot, D., Raffel, C., Roy, A., and Goodfellow, I. Understanding and improving interpolation in autoencoders via an adversarial regularizer. *arXiv preprint arXiv:1807.07543*, 2018.
- Cakir, E., Heittola, T., Huttunen, H., and Virtanen, T. Polyphonic sound event detection using multi label deep neural networks. In *2015 international joint conference on neural networks (IJCNN)*, pp. 1–7. IEEE, 2015.
- Cakir, E., Parascandolo, G., Heittola, T., Huttunen, H., and Virtanen, T. Convolutional recurrent neural networks for polyphonic sound event detection. *IEEE/ACM Transactions on Audio, Speech, and Language Processing*, 25(6):1291–1303, 2017.
- Cao, Y., Kong, Q., Iqbal, T., An, F., Wang, W., and Plumbley, M. D. Polyphonic sound event detection and localization using a two-stage strategy. *arXiv preprint arXiv:1905.00268*, 2019.
- Carter, S. and Nielsen, M. Using artificial intelligence to augment human intelligence. *Distill*, 2(12):e9, 2017.
- Chakrabarty, S. and Habets, E. A. Multi-speaker localization using convolutional neural network trained with noise. *arXiv preprint arXiv:1712.04276*, 2017.
- Chao, H., Zhi, H., Dong, L., and Liu, Y. Recognition of emotions using multichannel eeg data and dbn-gc-based ensemble deep learning framework. *Computational intelligence and neuroscience*, 2018, 2018.
- Chen, Y., Zheng, B., Zhang, Z., Wang, Q., Shen, C., and Zhang, Q. Deep learning on mobile and embedded devices: State-of-the-art, challenges, and future directions. *ACM Computing Surveys (CSUR)*, 53(4):1–37, 2020.
- Colombini, E. L., da Silva Simoes, A., and Ribeiro, C. *An attentional model for intelligent robotics agents*. PhD thesis, Instituto Tecnológico de Aeronáutica, São José dos Campos, Brazil, 2014.
- de Godoy, D., Islam, B., Xia, S., Islam, M. T., Chandrasekaran, R., Chen, Y.-C., Nirjon, S., Kinget, P. R., and Jiang, X. Paws: A wearable acoustic system for pedestrian safety. In *2018 IEEE/ACM Third International Conference on Internet-of-Things Design and Implementation (IoTDI)*, pp. 237–248. IEEE, 2018.
- DiBiase, J. H. *A high-accuracy, low-latency technique for talker localization in reverberant environments using microphone arrays*. Brown University, 2000.
- Dumoulin, V., Belghazi, I., Poole, B., Mastropietro, O., Lamb, A., Arjovsky, M., and Courville, A. Adversarially learned inference. *arXiv preprint arXiv:1606.00704*, 2016.
- Ferguson, E. L., Williams, S. B., and Jin, C. T. Sound source localization in a multipath environment using convolutional neural networks. In *2018 IEEE International Conference on Acoustics, Speech and Signal Processing (ICASSP)*, pp. 2386–2390. IEEE, 2018.
- Gao, J., Hu, M., Zhong, C., Li, G. Y., and Zhang, Z. An attention-aided deep learning framework for massive mimo channel estimation. *IEEE Transactions on Wireless Communications*, 21(3):1823–1835, 2021.
- Gupta, P. and Kar, S. Music and improved music algorithm to estimate direction of arrival. In *2015 International Conference on Communications and Signal Processing (ICCSP)*, pp. 0757–0761. IEEE, 2015.
- Ha, D. and Eck, D. A neural representation of sketch drawings. *arXiv preprint arXiv:1704.03477*, 2017.
- Hajavi, A. and Etemad, A. Knowing what to listen to: Early attention for deep speech representation learning. *arXiv preprint arXiv:2009.01822*, 2020.
- Hasan, M. K., Alam, M. A., Roy, S., Dutta, A., Jawad, M. T., and Das, S. Missing value imputation affects the performance of machine learning: A review and analysis of the literature (2010–2021). *Informatics in Medicine Unlocked*, 27:100799, 2021.
- He, K., Zhang, X., Ren, S., and Sun, J. Deep residual learning for image recognition. In *Proceedings of the IEEE conference on computer vision and pattern recognition*, pp. 770–778, 2016.

- Hirvonen, T. Classification of spatial audio location and content using convolutional neural networks. In *Audio Engineering Society Convention 138*. Audio Engineering Society, 2015.
- Hjelm, R. D., Fedorov, A., Lavoie-Marchildon, S., Grewal, K., Bachman, P., Trischler, A., and Bengio, Y. Learning deep representations by mutual information estimation and maximization. *arXiv preprint arXiv:1808.06670*, 2018.
- Hyadi, A., Rezki, Z., and Alouini, M.-S. An overview of physical layer security in wireless communication systems with csit uncertainty. *IEEE Access*, 4:6121–6132, 2016.
- Islam, B. I. and Nirjon, S. Zygarde: Time-sensitive on-device deep inference and adaptation on intermittently-powered systems. In *ACM Proceedings on Interactive, Mobile, Wearable and Ubiquitous Technologies (IMWUT/UBICOMP '20)*, Volume 4, Issue 3. ACM, 2020.
- Jerez, J. M., Molina, I., García-Laencina, P. J., Alba, E., Ribelles, N., Martín, M., and Franco, L. Missing data imputation using statistical and machine learning methods in a real breast cancer problem. *Artificial intelligence in medicine*, 50(2):105–115, 2010.
- Jiang, F., Fu, Y., Gupta, B. B., Liang, Y., Rho, S., Lou, F., Meng, F., and Tian, Z. Deep learning based multi-channel intelligent attack detection for data security. *IEEE transactions on Sustainable Computing*, 5(2):204–212, 2018.
- Lane, N. D., Bhattacharya, S., Mathur, A., Georgiev, P., Forlivesi, C., and Kawsar, F. Squeezing deep learning into mobile and embedded devices. *IEEE Pervasive Computing*, 16(3):82–88, 2017.
- Li, D., Wang, Y., Wang, J., Wang, C., and Duan, Y. Recent advances in sensor fault diagnosis: A review. *Sensors and Actuators A: Physical*, 309:111990, 2020a.
- Li, M., Liu, Y., Liu, X., Sun, Q., You, X., Yang, H., Luan, Z., Gan, L., Yang, G., and Qian, D. The deep learning compiler: A comprehensive survey. *IEEE Transactions on Parallel and Distributed Systems*, 32(3):708–727, 2020b.
- Lim, H., Park, J.-S., and Han, Y. Rare sound event detection using 1d convolutional recurrent neural networks. In *DCASE*, pp. 80–84, 2017.
- Little, R. J. and Rubin, D. B. *Statistical analysis with missing data*, volume 793. John Wiley & Sons, 2019.
- Ma, M., Ren, J., Zhao, L., Tulyakov, S., Wu, C., and Peng, X. Smil: Multimodal learning with severely missing modality. In *Proceedings of the AAAI Conference on Artificial Intelligence*, volume 35, pp. 2302–2310, 2021.
- Ma, M., Ren, J., Zhao, L., Testuggine, D., and Peng, X. Are multimodal transformers robust to missing modality? In *Proceedings of the IEEE/CVF Conference on Computer Vision and Pattern Recognition*, pp. 18177–18186, 2022.
- McAllester, D. and Stratos, K. Formal limitations on the measurement of mutual information. In *International Conference on Artificial Intelligence and Statistics*, pp. 875–884. PMLR, 2020.
- Mesaros, A., Heittola, T., Eronen, A., and Virtanen, T. Acoustic event detection in real life recordings. In *2010 18th European signal processing conference*, pp. 1267–1271. IEEE, 2010.
- Mesaros, A., Heittola, T., and Virtanen, T. Metrics for polyphonic sound event detection. *Applied Sciences*, 6(6):162, 2016.
- Noohi, T., Epain, N., and Jin, C. T. Direction of arrival estimation for spherical microphone arrays by combination of independent component analysis and sparse recovery. In *2013 IEEE International Conference on Acoustics, Speech and Signal Processing*, pp. 346–349. IEEE, 2013.
- Nugraha, A. A., Liutkus, A., and Vincent, E. Multichannel audio source separation with deep neural networks. *IEEE/ACM Transactions on Audio, Speech, and Language Processing*, 24(9):1652–1664, 2016.
- Orchard, T. and Woodbury, M. A. A missing information principle: theory and applications. In *Volume 1 Theory of Statistics*, pp. 697–716. University of California Press, 1972.
- Parascandolo, G., Huttunen, H., and Virtanen, T. Recurrent neural networks for polyphonic sound event detection in real life recordings. In *2016 IEEE international conference on acoustics, speech and signal processing (ICASSP)*, pp. 6440–6444. IEEE, 2016.
- Park, J., Woo, S., Lee, J.-Y., and Kweon, I. S. Bam: Bottleneck attention module. *arXiv preprint arXiv:1807.06514*, 2018.
- Phan, H., Hertel, L., Maass, M., and Mertins, A. Robust audio event recognition with 1-max pooling convolutional neural networks. *arXiv preprint arXiv:1604.06338*, 2016.
- Politis, A., Adavanne, S., Krause, D., Deleforge, A., Srivastava, P., and Virtanen, T. A dataset of dynamic reverberant sound scenes with directional interferers for sound event localization and detection. In *Proceedings of the 6th Detection and Classification of Acoustic Scenes and Events 2021 Workshop (DCASE2021)*, pp. 125–129, Barcelona, Spain, November 2021. ISBN 978-84-09-36072-7. URL <https://dcase.community/workshop2021/proceedings>.

- Poole, B., Ozair, S., Van Den Oord, A., Alemi, A., and Tucker, G. On variational bounds of mutual information. In Chaudhuri, K. and Salakhutdinov, R. (eds.), *Proceedings of the 36th International Conference on Machine Learning*, volume 97 of *Proceedings of Machine Learning Research*, pp. 5171–5180. PMLR, 09–15 Jun 2019. URL <https://proceedings.mlr.press/v97/poole19a.html>.
- Rahaman, A. and Kim, B. Microscale devices for biomimetic sound source localization: A review. *Journal of Microelectromechanical Systems*, 2021.
- Rajanna, A. R., Aryafar, K., Shokoufandeh, A., and Ptucha, R. Deep neural networks: A case study for music genre classification. In *2015 IEEE 14th international conference on machine learning and applications (ICMLA)*, pp. 655–660. IEEE, 2015.
- Roy, M. S., Roy, B., Gupta, R., and Sharma, K. D. On-device reliability assessment and prediction of missing photoplethysmographic data using deep neural networks. *IEEE transactions on biomedical circuits and systems*, 14(6):1323–1332, 2020.
- Roy, R. and Kailath, T. Esprit-estimation of signal parameters via rotational invariance techniques. *IEEE Transactions on acoustics, speech, and signal processing*, 37(7): 984–995, 1989.
- Rubin, D. B. Multiple imputation after 18+ years. *Journal of the American statistical Association*, 91(434):473–489, 1996.
- Sawada, H., Mukai, R., and Makino, S. Direction of arrival estimation for multiple source signals using independent component analysis. In *Seventh International Symposium on Signal Processing and Its Applications, 2003. Proceedings.*, volume 2, pp. 411–414. IEEE, 2003.
- Schmidt, R. Multiple emitter location and signal parameter estimation. *IEEE transactions on antennas and propagation*, 34(3):276–280, 1986.
- Schneider, S., Baevski, A., Collobert, R., and Auli, M. wav2vec: Unsupervised pre-training for speech recognition. *arXiv preprint arXiv:1904.05862*, 2019.
- Shimada, K., Koyama, Y., Takahashi, N., Takahashi, S., and Mitsufuji, Y. Accdoa: Activity-coupled cartesian direction of arrival representation for sound event localization and detection. In *ICASSP 2021-2021 IEEE International Conference on Acoustics, Speech and Signal Processing (ICASSP)*, pp. 915–919. IEEE, 2021.
- Taherian, H., Eskimez, S. E., Yoshioka, T., Wang, H., Chen, Z., and Huang, X. One model to enhance them all: array geometry agnostic multi-channel personalized speech enhancement. In *ICASSP 2022-2022 IEEE International Conference on Acoustics, Speech and Signal Processing (ICASSP)*, pp. 271–275. IEEE, 2022.
- Trowitzsch, I., Taghia, J., Kashef, Y., and Obermayer, K. The nigen general sound events database. *arXiv preprint arXiv:1902.08314*, 2019.
- Vergara, J. R. and Estévez, P. A. A review of feature selection methods based on mutual information. *Neural computing and applications*, 24(1):175–186, 2014.
- Virtanen, T., Plumbley, M. D., and Ellis, D. *Computational analysis of sound scenes and events*. Springer, 2018.
- Xiao, X., Zhao, S., Zhong, X., Jones, D. L., Chng, E. S., and Li, H. A learning-based approach to direction of arrival estimation in noisy and reverberant environments. In *2015 IEEE International Conference on Acoustics, Speech and Signal Processing (ICASSP)*, pp. 2814–2818. IEEE, 2015.
- Yalta, N., Nakadai, K., and Ogata, T. Sound source localization using deep learning models. *Journal of Robotics and Mechatronics*, 29(1):37–48, 2017.
- Yang, Z., Li, J., Stoica, P., and Xie, L. Sparse methods for direction-of-arrival estimation. In *Academic Press Library in Signal Processing, Volume 7*, pp. 509–581. Elsevier, 2018.
- Yin, Z. and Hou, J. Recent advances on svm based fault diagnosis and process monitoring in complicated industrial processes. *Neurocomputing*, 174:643–650, 2016.
- Yiwere, M. and Rhee, E. J. Distance estimation and localization of sound sources in reverberant conditions using deep neural networks. *Int. J. Appl. Eng. Res.*, 12(22): 12384–12389, 2017.
- Yuan, Y., Xun, G., Ma, F., Suo, Q., Xue, H., Jia, K., and Zhang, A. A novel channel-aware attention framework for multi-channel eeg seizure detection via multi-view deep learning. In *2018 IEEE EMBS International Conference on Biomedical & Health Informatics (BHI)*, pp. 206–209. IEEE, 2018.
- Zhang, H., McLoughlin, I., and Song, Y. Robust sound event recognition using convolutional neural networks. In *2015 IEEE international conference on acoustics, speech and signal processing (ICASSP)*, pp. 559–563. IEEE, 2015.